

Article

# Low-Symmetry Phthalocyanines Bearing Carboxy-Groups: Synthesis, Spectroscopic and Quantum-Chemical Characterization

Dmitry A. Bunin<sup>1</sup>, Nobuhle Ndebele<sup>2</sup>, Alexander G. Martynov<sup>1</sup>, John Mack<sup>2</sup> , Yulia G. Gorbunova<sup>1,3,\*</sup>   
and Tebello Nyokong<sup>2,\*</sup> 

<sup>1</sup> A. N. Frumkin Institute of Physical Chemistry and Electrochemistry, Russian Academy of Sciences, Leninsky pr., 31, Building 4, 119071 Moscow, Russia; bunin\_dm@mail.ru (D.A.B.); martynov@phyche.ac.ru (A.G.M.)

<sup>2</sup> Institute for Nanotechnology Innovation, Department of Chemistry, Rhodes University, Makhanda 6140, South Africa; g13n7164@campus.ru.ac.za (N.N.); j.mack@ru.ac.za (J.M.)

<sup>3</sup> N. S. Kurnakov Institute of General and Inorganic Chemistry, Russian Academy of Sciences, Leninsky pr., 31, 119991 Moscow, Russia

\* Correspondence: yulia@igic.ras.ru (Y.G.G.); t.nyokong@ru.ac.za (T.N.)

**Abstract:** The synthesis and characterization of A<sub>3</sub>B-type phthalocyanines, **ZnPc1–4**, bearing bulky 2,6-diisopropylphenoxy-groups or chlorine atoms on isoindoline units “A” and either one or two carboxylic anchors on isoindoline unit “B” are reported. A comparison of molecular modelling with the conventional time dependent—density functional theory (TD-DFT) approach and its simplified sTD-DFT approximation provides further evidence that the latter method accurately reproduces the key trends in the spectral properties, providing colossal savings in computer time for quite large molecules. This demonstrates that it is a valuable tool for guiding the rational design of new phthalocyanines for practical applications.

**Keywords:** phthalocyanine; UV-vis spectroscopy; MCD spectroscopy; TD-DFT



**Citation:** Bunin, D.A.; Ndebele, N.; Martynov, A.G.; Mack, J.; Gorbunova, Y.G.; Nyokong, T. Low-Symmetry Phthalocyanines Bearing Carboxy-Groups: Synthesis, Spectroscopic and Quantum-Chemical Characterization. *Molecules* **2022**, *27*, 524. <https://doi.org/10.3390/molecules27020524>

Academic Editor: Vladimir Burilov

Received: 13 December 2021

Accepted: 12 January 2022

Published: 14 January 2022

**Publisher’s Note:** MDPI stays neutral with regard to jurisdictional claims in published maps and institutional affiliations.



**Copyright:** © 2022 by the authors. Licensee MDPI, Basel, Switzerland. This article is an open access article distributed under the terms and conditions of the Creative Commons Attribution (CC BY) license (<https://creativecommons.org/licenses/by/4.0/>).

## 1. Introduction

Phthalocyanines (Pcs) are macrocyclic ligands of particular interest because of their high stability, excellent photophysical properties and facile structural modification, which can readily be used to control the properties of corresponding materials and devices [1–3]. From this standpoint, low-symmetry Pcs are particularly interesting since combining various functional groups at the ligand periphery enables a rational modulation of their properties such as solubility, compatibility with nanomaterials, and nonlinear optical properties [4]. For example, low-symmetry Pcs bearing one or two carboxylic groups can act as the light-harvesting components of dye-sensitized solar cells (DSSCs) when these sensitizers are grafted on the surface of TiO<sub>2</sub> or ZnO [5]. To control the aggregation and solubility of these Pcs, bulky groups can be introduced varying from relatively small *tert*-butyl groups [6] to perfluoro-*tert*-butyl substituents [7] and sterically demanding 2,6-disubstituted phenoxy-groups [8–11]. Moreover, carboxy-substituted Pcs can be conjugated with various nanomaterials, such as gold nanoparticles [12] or carbon nanotubes [13] to provide photoactive hybrid materials.

In addition to the control of aggregation, the substitution pattern should also help to align the frontier orbital energies of the sensitizer and the conduction band of metal oxides, so molecular modelling calculations can be used to guide further synthetic work in a rational manner [14] and improve device performance [15,16]. The accurate prediction of UV-visible absorption (UV-vis) spectra of low-symmetry Pc sensitizers is critical since photon absorption is the primary act in the sequence of physical processes that convert solar energy into electricity. Typically, this task is solved using the time dependent—density functional theory (TD-DFT) method [17–20], although the relatively high computational

cost can limit its applicability in the context of large molecules with sterically demanding substituents. In this study, the synthesis of a series of zinc phthalocyanines, **ZnPc1–4**, with bulky solubilizing diisopropylphenoxy-groups and either one or two carboxylic anchors is reported (Figure 1). Analyses of their UV-vis spectra using the classical TD-DFT approach and its simplified approximation (sTD-DFT) [21,22], demonstrate that the latter approach provides a spectacular speed-up of calculations by orders of magnitude, which is particularly useful in the theoretical treatment of large conjugated molecules such as phthalocyanines [22–25].

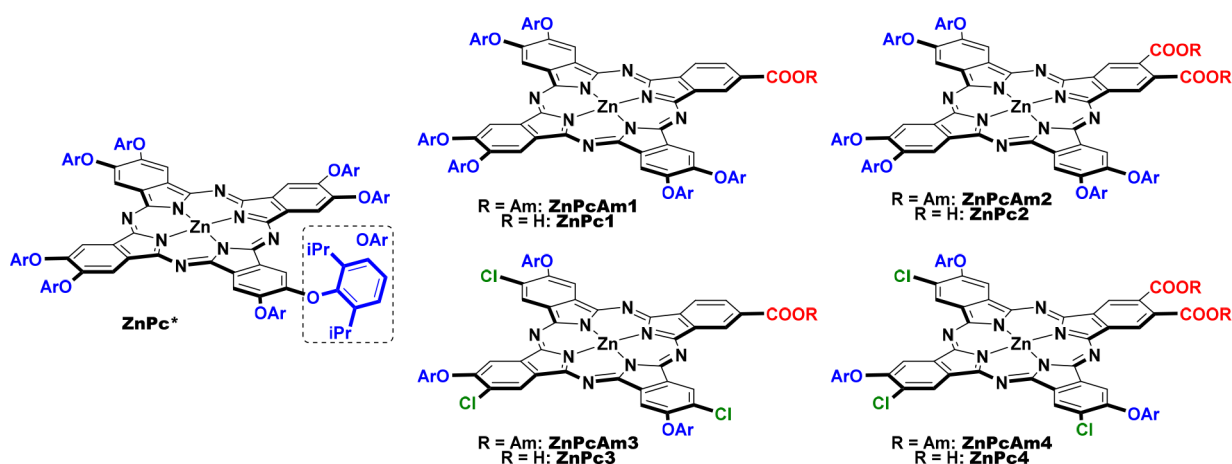
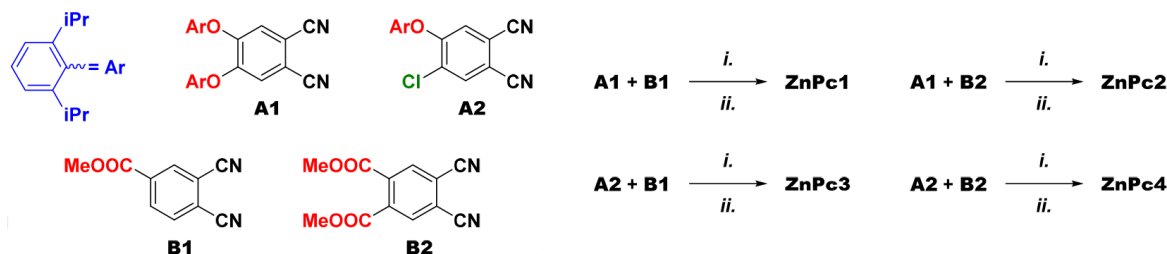


**Figure 1.** The structures of symmetrical reference complex **ZnPc\*** and  $A_3B$ -type zinc phthalocyanines **ZnPc1–4** synthesized in this work. The amyl esters **ZnPcAm1–4** were obtained as intermediates in the synthesis of the corresponding **ZnPc1–4**.

## 2. Results

Carboxy-substituted Pcs can be synthesized by a cross-condensation template reaction of phthalonitriles bearing bulky solubilizing groups and those functionalized either with hydroxymethyl or ester groups followed by chromatographic isolation of the low-symmetry target complexes. The  $CH_2OH$ -substituted complexes can then be oxidized using iodoxybenzoic acid to form an aldehyde followed by oxidation to form a  $-COOH$  group by using  $NaClO_2$  in the presence of sulfamic acid [6,26,27]. Recently, direct oxidation of  $Zn[(tBu)_3(CH_2OH)Pc]$  to the corresponding carboxy-substituted complex was reported; the anaerobic reaction of the specified complex with  $KOH$  catalyzed by  $ZnO$  furnished the well-known **TT1** dye [28]. Ester-substituted Pcs can be hydrolyzed to form target complexes bearing  $-COOH$  groups [8,9]. This method was selected for use in this study (Scheme 1).



**Scheme 1.** Synthesis of zinc phthalocyanines **ZnPc1–4**: *i.*— $Zn(OAc)_2$ , 1,8-diazabicyclo[5.4.0]undec-7-ene, *n*-pentanol; *ii.*— $NaOH$ ,  $H_2O$ , tetrahydrofuran,  $MeOH$ .

Synthesis of  $A_3B$ -Pcs was performed from the previously reported precursors—4,5-bis(2,6-diisopropylphenoxy)- or 4-chloro-5-(2,6-diisopropylphenoxy)-substituted phthalonitriles **1** and **2** for the A ring moieties, and methyl-3,4-dicyanobenzoate **3** or dimethyl-4,5-

dicyanophthalate **4** on the B ring moieties. Condensation of the corresponding pairs of precursors in refluxing *n*-pentanol in the presence of Zn(OAc)<sub>2</sub> and DBU afforded mixtures containing mainly the A<sub>4</sub>, A<sub>3</sub>B and A<sub>2</sub>B<sub>2</sub> macrocyclic products. Because of transesterification, methyl groups were replaced by amyl residues, which decreased the overall polarity of the resulting complexes and hampered chromatographic separation of the A<sub>3</sub>B product from the A<sub>4</sub> and A<sub>2</sub>B<sub>2</sub> structures. Hydrolysis of ester bonds in ZnPcAm1–4 resulted in the formation of the acid groups of the target compounds, which can be readily separated, from traces of the relatively nonpolar A<sub>4</sub> and the much more polar A<sub>2</sub>B<sub>2</sub> derivatives. Control over the separation was achieved by thin-layer chromatography (TLC) and matrix-assisted laser desorption ionization-time-of-flight (MALDI-TOF) mass spectrometry. All complexes isolated were characterized by UV-vis and <sup>1</sup>H NMR spectroscopy (See Supplementary Materials).

The UV-vis and magnetic circular dichroism (MCD) spectra of ZnPc1–4 (Figure 2) were measured in DMF to suppress their aggregation properties so the spectral properties of the monomeric complexes can be compared with those of ZnPc\*, a fully symmetric A<sub>4</sub> compound with sterically demanding substituents that was isolated as a byproduct during the synthesis of ZnPc1 and ZnPc2. The introduction of electron-withdrawing carboxy-groups and/or chlorine atoms has only a relatively minor effect on the Q-band wavelengths, resulting in a bathochromic shift of up to 7 nm relative to that of the symmetric ZnPc\* reference compound.

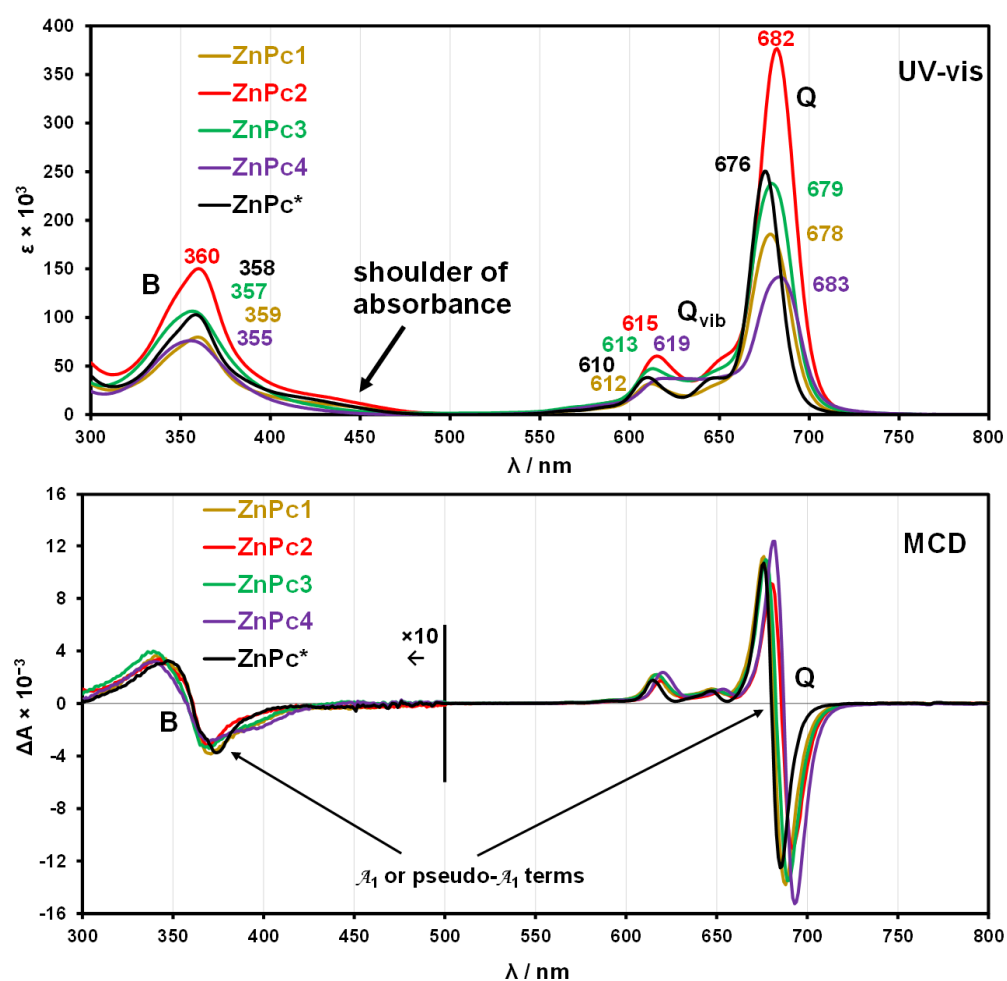


**Figure 2.** UV-visible absorption and magnetic circular dichroism (MCD) spectra of the zinc phthalocyaninates in dimethylformamide. MCD spectra were measured for solutions with a fixed Q<sub>00</sub> band absorbance of 1.4.

The effect of introducing the peripheral substituents was analyzed through a comparison of the experimental spectral data with the TD-DFT and sTD-DFT calculations. In contrast to previous studies of substituted phthalocyanines where bulky alkoxy and aryloxy groups were truncated and replaced with methoxy groups to save computational time [22–25], in the present work, all calculations were performed for molecules with genuine diisopropylphenoxy substituents to further demonstrate the capabilities of the sTD-DFT approach in the context of a desktop computer.

The optical properties of porphyrinoid complexes, such as phthalocyanines, can be readily conceptualized through a consideration of the molecular orbitals (MOs) associated with the 16 atom 18  $\pi$ -electron inner ligand perimeter that have an  $M_L = 0, \pm 1, \pm 2, \pm 3, \pm 4, \pm 5, \pm 6, \pm 7, 8$  sequence in ascending energy terms [29,30]. The highest occupied molecular orbital (HOMO) and lowest unoccupied molecular orbital (LUMO) have  $M_L = \pm 4$  and  $\pm 5$  angular nodal patterns, respectively, resulting in Q and B bands with  $\Delta M_L = \pm 1$  and  $\pm 9$  properties at lower and higher energy. Michl [30] introduced an **a**, **s**, **-a** and **-s** nomenclature for the MOs derived from the four frontier  $\pi$ -MOs of a  $C_{16}H_{16}^{2-}$  parent perimeter (Figure 3), depending on whether there are nodal planes (**a**/**-a**) and MO coefficients (**s**/**-s**) aligned with the *y*-axis, which enables the facile comparison of the electronic structures of cyclic polyenes of differing symmetry. In the context of phthalocyanines, the peripheral benzo ring substitution introduces a second frontier  $\pi$ -MO with  $a_{2u}$  symmetry [29,31–33] that complicates the analysis of the electronic structures of phthalocyanines (Figure 4).

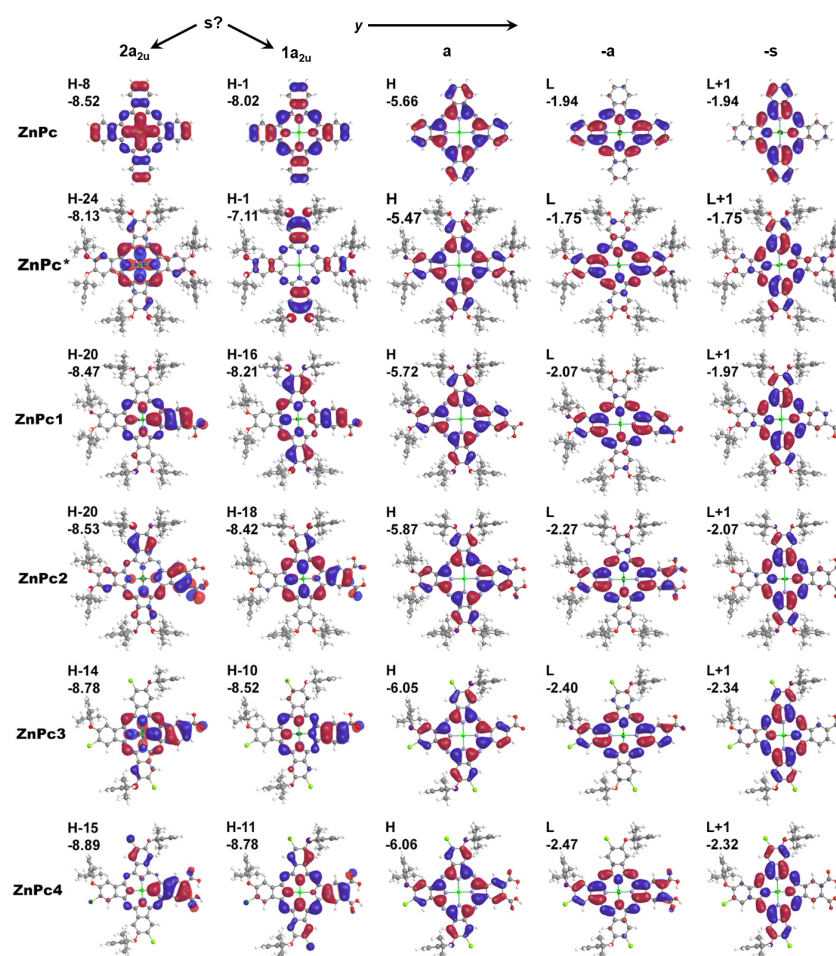


**Figure 3.** Nodal structure and energies (eV) of frontier orbitals in ZnPc\* and ZnPc1–4 according to CAM-B3LYP/6-31G(d) calculations.

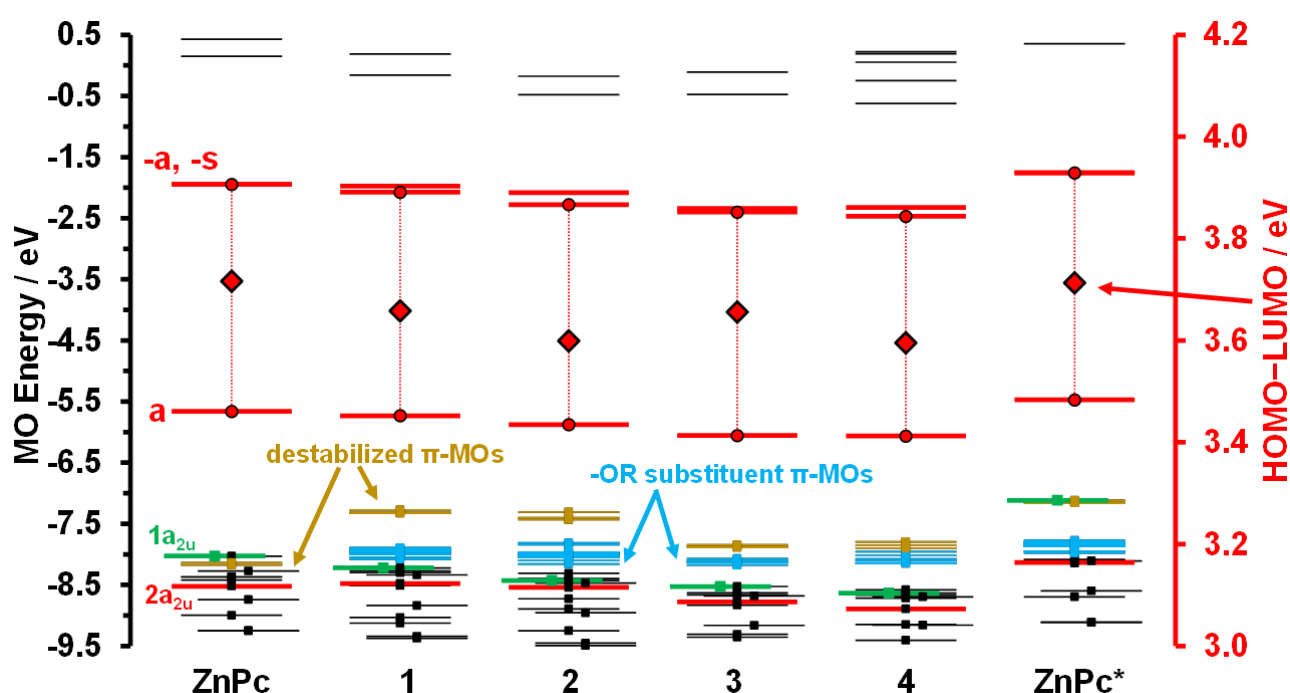


**Figure 4.** Molecular orbital (MO) energies of ZnPc, ZnPc\* and ZnPc1–4. The a, s ( $2a_{2u}$ ), -a and -s MOs are highlighted in red with circles used to denote the a and -a MOs, while green is used to highlight MOs derived from the  $1a_{2u}$  MO of ZnPc. The occupied MOs are highlighted with small squares. MOs localized on the sterically demanding -OR substituents are highlighted in light blue, while amber is used for  $\pi$ -MOs localized on the peripheral benzo rings that are destabilized. Red diamonds are used to highlight the highest occupied molecular orbital–lowest unoccupied molecular orbital (HOMO–LUMO) gap values and are plotted against a secondary axis.  $\sigma$ -MOs associated with the aza-nitrogen lone pairs are offset to the right.

Spectral band deconvolution studies for a series of axially ligated Zn<sup>II</sup>Pc complexes by Nyokong and coworkers identified the presence of two intense overlapping Faraday  $A_1$  terms in the B band region [34] that were subsequently labelled as the  $B_1$  and  $B_2$  bands [4,35–40]. These bands can be assigned primarily to the  $1a_{2u} \rightarrow -a/-s$  and  $1b_{2u} \rightarrow -a/-s$  one-electron transitions on the basis of the molecular modelling at the B3LYP/6-31G(d) level of theory (Tables 1 and 2). For this reason, the  $1a_{2u}$  MO (Figure 3) has previously been assumed to be the s MO of ZnPc in the context of Michl’s perimeter model [4,22,33,41].

The assignment of the higher energy  $\pi\pi^*$  transitions of ZnPc1–4 and ZnPc\* in the B band region is problematic due to the complicated configurational interaction that is predicted, but broadly similar trends are predicted in the TD-DFT and sTD-DFT calculations (Figure 5, Tables 1 and 2). An extra intense band is predicted in the 300–400 nm region in the sTD-DFT calculations for ZnPc1–4 and ZnPc\* and in the TD-DFT calculations for ZnPc1, ZnPc2 and ZnPc\* (Figure 5) due to the mesomeric effects of the oxygen lone pairs of the peripheral substituents on MOs that are localized primarily on the peripheral benzo rings. A marked destabilization is predicted for these MOs, which includes the  $1a_{2u}$  MO in the context of ZnPc\* (Figures 4 and 5, Tables 1 and 2). It is hence reasonable to conclude that the  $2a_{2u} \rightarrow -a/-s$  one-electron transitions are likely to dominate in the context of the main B band of ZnPc\* as is predicted in the TD-DFT and sTD-DFT calculations (Figure 5, Tables 1 and 2).

**Table 1.** The calculated gas-phase UV-vis absorption spectra for the B3LYP geometries calculated for the Q and B bands by the conventional TD-DFT method at the CAM-B3LYP/6-31G(d) level of theory.

	$\lambda_{\chi\alpha\lambda\chi'} \nu\mu$ (eV)	$f_{\text{calc}}$	Q Band Wavefunctions <sup>a</sup>	$\lambda_{\chi\alpha\lambda\chi'} \nu\mu$ (eV)	$f_{\text{calc}}$	Wavefunctions of the Most Intense Bands Predicted in the B Band Region <sup>a</sup>
ZnPc	607 (2.04)	0.48	94% a → -a; ...	313 (3.96)	0.02	70% H-2 (1b <sub>2u</sub> ) <sup>Bz</sup> → -a; 20% 2a <sub>2u</sub> → -a; ...
	607 (2.04)	0.48	94% a → -s; ...	313 (3.96)	0.02	70% H-2 (1b <sub>2u</sub> ) <sup>Bz</sup> → -s; 20% 2a <sub>2u</sub> → -s; ...
				295 (4.21)	1.07	74% 1a <sub>2u</sub> <sup>Bz</sup> → -a/-s; 9% 2a <sub>2u</sub> → -a/-s; 7% a → -a/-s; ...
				295 (4.21)	1.07	74% 1a <sub>2u</sub> <sup>Bz</sup> → -a/-s; 9% 2a <sub>2u</sub> → -a/-s; 7% a → -a/-s; ...
ZnPc*	622 (1.99)	0.56	92% a → -a; ...	366 (3.39)	0.04	73% H-1 (1b <sub>2u</sub> ) <sup>Bz</sup> → -a; ...
	622 (1.99)	0.56	92% a → -s; ...	366 (3.39)	0.04	87% H-2 (1b <sub>2u</sub> ) <sup>Bz</sup> → -a; ...
				332 (3.74)	0.95	75% 1a <sub>2u</sub> <sup>Bz</sup> → -a; 18% H-2 (1b <sub>2u</sub> ) <sup>Bz</sup> → -a; ...
				332 (3.74)	0.95	72% 1a <sub>2u</sub> <sup>Bz</sup> → -s; 21% H-2 (1b <sub>2u</sub> ) <sup>Bz</sup> → -s; ...
				295 (4.20)	0.6	66% 2a <sub>2u</sub> → -s; 10% H-25 (1b <sub>1u</sub> ) → -a; ...
			295 (4.20)	0.6	66% 2a <sub>2u</sub> → -a; 10% H-25 (1b <sub>1u</sub> ) → -s; ...	
ZnPc1	626 (1.98)	0.53	93% a → -s; ...	372 (3.33)	0.08	83% H-1 <sup>Bz</sup> → -s; ...
	613 (2.02)	0.58	92% a → -a; ...	346 (3.58)	0.54	83% H-1 <sup>Bz</sup> → -a; ...
				342 (3.63)	0.16	73% H-2 <sup>Bz</sup> → -a; ...
				333 (3.72)	0.34	57% H-3 <sup>Bz</sup> → -s; 19% a → L+2 (1b <sub>1u</sub> <sup>*</sup> ); ...
				327 (3.79)	0.11	69% a → L+2 (1b <sub>1u</sub> <sup>*</sup> ); 20% H-3 <sup>Bz</sup> → -s; ...
				311 (3.88)	0.17	63% a → L+3 (1b <sub>2u</sub> <sup>*</sup> ); 14% 1a <sub>2u</sub> <sup>Bz</sup> → -a/-s; ...
				304 (4.08)	0.3	51% 1a <sub>2u</sub> <sup>Bz</sup> → -a/-s; 14% a → L+3 (1b <sub>2u</sub> <sup>*</sup> ); ...
				299 (4.15)	0.49	38% 2a <sub>2u</sub> → -a; 15% H-17 (2e <sub>g</sub> ) → -a/-s; 8% 1a <sub>2u</sub> <sup>Bz</sup> → -a/-s; ...
			298 (4.17)	0.58	27% 2a <sub>2u</sub> → -a/-s; 18% H-18 (1b <sub>1u</sub> ) → -a/-s; 11% 1a <sub>2u</sub> <sup>Bz</sup> → -s; ...	
			286 (4.33)	0.13	35% H-18 (1b <sub>1u</sub> ) → -a; 14% H-17 (2e <sub>g</sub> ) → -a/-s; 11% 1a <sub>2u</sub> <sup>Bz</sup> → -s;	
ZnPc2	636 (1.95)	0.57	94% a → -a; ...	378 (3.28)	0.09	67% H-2 <sup>Bz</sup> → -a/-s; 19% H-1 <sup>Bz</sup> → -s; ...
	607 (2.04)	0.56	93% a → -s; ...	357 (3.47)	0.4	88% H-1 <sup>Bz</sup> → -a/-s; ...
				348 (3.56)	0.17	85% H-2 <sup>Bz</sup> → -a/-s; ...
				345 (3.62)	0.15	76% a → L+3 (1b <sub>2u</sub> <sup>*</sup> ); 10% H-3 <sup>Bz</sup> → -s; ...
				331 (3.74)	0.32	60% H-3 <sup>Bz</sup> → -s; 20% a → L+3 (1b <sub>2u</sub> <sup>*</sup> ); ...
				306 (4.05)	0.71	34% 1a <sub>2u</sub> <sup>Bz</sup> → -a; 31% H-16 (2e <sub>g</sub> ) → -a/-s; ...
				303 (4.09)	0.59	40% H-17 (1b <sub>1u</sub> ) → -a/-s; 19% 1a <sub>2u</sub> <sup>Bz</sup> → -s; ...
				288 (4.30)	0.22	38% 1a <sub>2u</sub> <sup>Bz</sup> → -a/-s; 17% H-17 (1b <sub>1u</sub> ) → -a/-s; 7% 2a <sub>2u</sub> → -a/-s; ...
			286 (4.34)	0.13	44% 1a <sub>2u</sub> <sup>Bz</sup> → -a/-s; ...	

Table 1. Cont.

	$\lambda_{\chi\alpha\lambda\chi'} \nu\mu$ (eV)	$f_{\text{calc}}$	Q Band Wavefunctions <sup>a</sup>	$\lambda_{\chi\alpha\lambda\chi'} \nu\mu$ (eV)	$f_{\text{calc}}$	Wavefunctions of the Most Intense Bands Predicted in the B Band Region <sup>a</sup>
ZnPc3	624 (1.99) 616 (2.01)	0.53 0.61	<b>93% a</b> → -s; ... <b>92% a</b> → -a; ...	350 (3.54)	0.06	49% H-1 <sup>Bz</sup> → -s; 25% H-2 <sup>Bz</sup> → -a/-s; ...
				326 (3.80)	0.51	34% H-1 <sup>Bz</sup> → -a; 19% H-3 <sup>Bz</sup> → -a; 12% H-2 <sup>Bz</sup> → -a; ...
				315 (3.93)	0.48	79% H-3 <sup>Bz</sup> → -s; ...
				309 (4.01)	0.5	<b>38% 1a<sub>2u</sub><sup>Bz</sup></b> → -a; 26% a → L+3 (1b <sub>2u</sub> <sup>*</sup> ); ...
				303 (4.09)	0.14	53% a → L+3 (1b <sub>2u</sub> <sup>*</sup> ); <b>26% 1a<sub>2u</sub><sup>Bz</sup></b> → -a/-s; ...
				298 (4.16)	0.7	<b>31% 1a<sub>2u</sub><sup>Bz</sup></b> → -a/-s; <b>20% 2a<sub>2u</sub></b> → -a/-s; 10% H-12 (1b <sub>1u</sub> <sup>*</sup> ) → -a; ...
				297 (4.19)	0.45	<b>46% 2a<sub>2u</sub></b> → -a/-s; 12% H-12 (1b <sub>1u</sub> <sup>*</sup> ) → -a/-s; <b>11% 1a<sub>2u</sub><sup>Bz</sup></b> → -a/-s; ...
ZnPc4	635 (1.95) 612 (2.03)	0.61 0.58	<b>94% a</b> → -s; ... <b>94% a</b> → -a; ...	353 (3.51)	0.08	40% H-2 <sup>Bz</sup> → -s; 30% H-1 <sup>Bz</sup> → -s; ...
				337 (3.67)	0.07	72% a → L+2 (1b <sub>1u</sub> <sup>*</sup> ); ...
				332 (3.74)	0.48	80% H-1 <sup>Bz</sup> → -a; ...
				328 (3.78)	0.1	65% H-2 <sup>Bz</sup> → -a; ...
				316 (3.93)	0.17	81% a → L+3 (1b <sub>2u</sub> <sup>*</sup> ); ...
				314 (3.95)	0.46	80% H-3 <sup>Bz</sup> → -s; ...
				302 (4.11)	0.64	33% H-10 (2e <sub>g</sub> ) → -a; <b>31% 1a<sub>2u</sub><sup>Bz</sup></b> → -a; ...
299 (4.14)	0.56	<b>21% 2a<sub>2u</sub></b> → -a/-s; <b>19% 1a<sub>2u</sub><sup>Bz</sup></b> → -s; 13% H-10 (2e <sub>g</sub> ) → -a/-s; 12% H-12 (1b <sub>1u</sub> ) → -a/-s; ...				
298 (4.16)	0.24	<b>25% 2a<sub>2u</sub></b> → -a/-s; 16% H-12 (1b <sub>1u</sub> ) → -a/-s; <b>13% 1a<sub>2u</sub><sup>Bz</sup></b> → -s; ...				

a—The wavefunctions based on the eigenvectors predicted in conventional TD-DFT calculations. One-electron transitions associated with the **a**, **-a** and **-s** MOs and the two frontier MOs derived from the 1a<sub>2u</sub> and 2a<sub>2u</sub> MOs of ZnPc that could potentially be viewed as the s MO are highlighted in bold. Only contributions > 10% to transitions with  $f > 0.10$  and  $\lambda > 285$  nm are consistently included. Bz as a superscript denotes an MO that is mainly localized on the peripheral benzo rings. Italics are used for other bands in the B band region (285–400 nm) that are not assigned to the main electronic B transitions in Figure 5. Where appropriate, the ZnPc MO from which the MO is derived is provided in parentheses.

**Table 2.** The calculated gas-phase UV-vis absorption spectra for the B3LYP geometries calculated for the Q and B bands by the sTD-DFT method at the CAM-B3LYP/6-31G(d) level of theory.

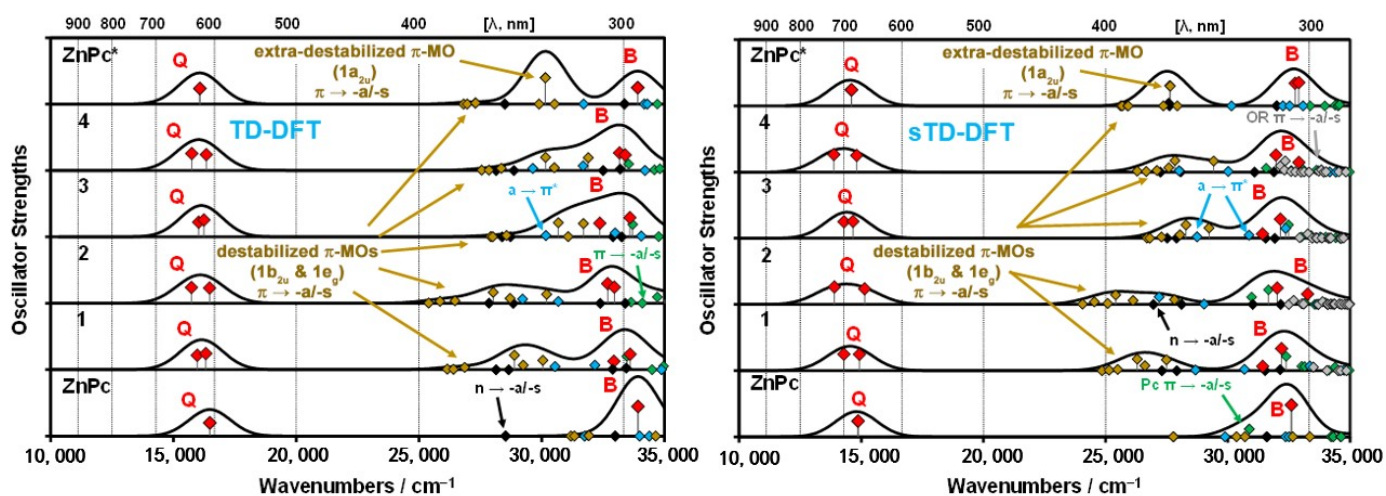
	$\lambda_{\chi\alpha\lambda\chi'} \nu\mu$ (eV)	$f_{\text{calc}}$	Q Band Wavefunctions <sup>a</sup>	$\lambda_{\chi\alpha\lambda\chi'} \nu\mu$ (eV)	$f_{\text{calc}}$	Wavefunctions of the Most Intense Bands Predicted in the B Band Region <sup>a</sup>
<b>ZnPc</b>	676 (1.84)	0.57	97% a → -a/-s; ...	325 (3.81)	0.28	74% H-2 (1b <sub>2u</sub> ) → -a; 14% s → -a; ...
	675 (1.84)	0.57	97% a → -s/-a; ...	325 (3.81)	0.28	74% H-2 (1b <sub>2u</sub> ) → -s; 14% s → -s; ...
				308 (4.03)	1.16	79% 1a <sub>2u</sub> <sup>Bz</sup> → -a; 9% H-2 (1b <sub>2u</sub> ) → -a; ...
				308 (4.03)	1.16	74% 1a <sub>2u</sub> <sup>Bz</sup> → -s; 9% H-2 (1b <sub>2u</sub> ) → -s; ...
<b>ZnPc*</b>	689 (1.80)	0.59	95% a → -a/-s; ...	364 (3.41)	0.63	70% 1a <sub>2u</sub> <sup>Bz</sup> → -a/-s; H-2 (1b <sub>2u</sub> ) → -a; ...
	688 (1.80)	0.59	95% a → -s/-a; ...	364 (3.41)	0.64	71% 1a <sub>2u</sub> <sup>Bz</sup> → -a/-s; 9% H-2 (1b <sub>2u</sub> ) → -s; ...
				363 (3.41)	0.18	58% H-18 (1b <sub>2g</sub> <sup>N</sup> ) → -s; 18% 1a <sub>2u</sub> <sup>Bz</sup> → -s; 13% H-1 <sup>OAr</sup> → -s; ...
				363 (3.41)	0.12	61% H-18 (1b <sub>2g</sub> <sup>N</sup> ) → -s; 14% H-14 <sup>OAr</sup> → -s; 13% 1a <sub>2u</sub> <sup>Bz</sup> → -s; ...
				307 (4.04)	0.85	62% 2a <sub>2u</sub> → -a; 16% H-25 (1b <sub>1u</sub> ) → -s; ...
				307 (4.04)	0.85	61% 2a <sub>2u</sub> → -s; 16% H-25 (1b <sub>1u</sub> ) → -a; ...
<b>ZnPc1</b>	703 (1.76)	0.6	97% a → -a; ...	382 (3.25)	0.42	80% H-1 <sup>Bz</sup> → -a; ...
	673 (1.84)	0.59	96% a → -s; ...	377 (3.29)	0.17	82% H-2 <sup>Bz</sup> → -a/-s; ...
				365 (3.39)	0.39	75% H-3 <sup>Bz</sup> → -s; ...
				320 (3.88)	0.16	57% 1a <sub>2u</sub> <sup>Bz</sup> → -a; 9% 2a <sub>2u</sub> → -a; 15% a → L+3 (1b <sub>2u</sub> <sup>*</sup> ); ...
				312 (3.98)	0.8	26% H-18 (1b <sub>1u</sub> ) → -a; 25% 1a <sub>2u</sub> <sup>Bz</sup> → -s; ...
				310 (4.00)	0.51	58% 2a <sub>2u</sub> → -a; 12% H-18 (1b <sub>1u</sub> ) → -s; ...
				304 (4.08)	0.16	31% H-17 (2e <sub>g</sub> ) → -a; 27% a → L+4 (1a <sub>2u</sub> <sup>*</sup> ); ...
				303 (4.09)	0.15	45% H-17 (2e <sub>g</sub> ) → -s; 24% a → L+4 (1a <sub>2u</sub> <sup>*</sup> ); ...
				301 (4.12)	0.16	40% H-17 (2e <sub>g</sub> ) → -a/-s; 37% a → L+4 (1a <sub>2u</sub> <sup>*</sup> ); ...
				300 (4.14)	0.13	33% 1a <sub>2u</sub> <sup>Bz</sup> → -s; 29% H-18 (1b <sub>1u</sub> ) → -a; ...
			292 (4.25)	0.13	40% H-20 (2e <sub>g</sub> ) → -a; 30% 2a <sub>2u</sub> → -s; ...	
<b>ZnPc2</b>	723 (1.72)	0.64	97% a → -a; ...	395 (3.14)	0.35	86% H-1 <sup>Bz</sup> → -a/-s; ...
	663 (1.87)	0.57	97% a → -s; ...	384 (3.23)	0.14	84% H-2 <sup>Bz</sup> → -a/-s; ...
				369 (3.36)	0.27	52% a → L+2 (1b <sub>1u</sub> <sup>*</sup> ); 38% H-3 <sup>Bz</sup> → -s; ...
				361 (3.43)	0.17	45% H-3 <sup>Bz</sup> → -s; 36% a → L+2 (1b <sub>1u</sub> <sup>*</sup> ); ...
				324 (3.82)	0.27	57% H-16 (2e <sub>g</sub> ) → -a; ...
				317 (3.91)	0.53	51% H-11 (1b <sub>1u</sub> ) → -a; 51% H-10 <sup>OAr</sup> → -a; 9% 1a <sub>2u</sub> <sup>Bz</sup> → -s; ...
				314 (3.95)	0.6	42% 1a <sub>2u</sub> <sup>Bz</sup> → -a; 14% 2a <sub>2u</sub> → -a; 10% H-21 (2e <sub>g</sub> ) → -a; ...
				307 (4.04)	0.15	54% H-4 <sup>OAr</sup> → -a/-s; 18% 1a <sub>2u</sub> <sup>Bz</sup> → -s; ...

Table 2. Cont.

	$\lambda_{\chi\alpha\lambda\chi'} \nu\mu$ (eV)	$f_{\text{calc}}$	Q Band Wavefunctions <sup>a</sup>	$\lambda_{\chi\alpha\lambda\chi'} \nu\mu$ (eV)	$f_{\text{calc}}$	Wavefunctions of the Most Intense Bands Predicted in the B Band Region <sup>a</sup>
ZnPc3	703 (1.76) 685 (1.81)	0.6 0.62	97% a → -s; ... 97% a → -a; ...	302 (4.11)	0.38	40% 2a <sub>2u</sub> → -s; 10% H-4 <sup>OAr</sup> → -s; ...
				296 (4.18)	0.1	20% H-4 <sup>OAr</sup> → -s; 15% H-10 <sup>OAr</sup> → -a; 12% H-17 (1b <sub>1u</sub> ) → -s; ...
				358 (3.46)	0.13	42% H-1 <sup>Bz</sup> → -a; 23% H-2 <sup>Bz</sup> → -a; 20% a → L+2 (1b <sub>1u</sub> <sup>*</sup> ); ...
				355 (3.49)	0.48	35% H-3 <sup>Bz</sup> → -a; 21% H-1 <sup>Bz</sup> → -a; 19% H-2 <sup>Bz</sup> → -a; ...
				344 (3.61)	0.38	75% H-3 <sup>Bz</sup> → -s; 15% a → L+2 (1b <sub>1u</sub> <sup>*</sup> ); ...
				325 (3.81)	0.11	76% a → L+3 (1b <sub>2u</sub> <sup>*</sup> ); 7% 1a <sub>2u</sub> <sup>Bz</sup> → -a; ...
				320 (3.88)	0.16	49% 1a <sub>2u</sub> <sup>Bz</sup> → -a; 16% 2a <sub>2u</sub> → -a; 15% a → L+3 (1b <sub>2u</sub> <sup>*</sup> ); ...
				312 (3.97)	0.69	36% 1a <sub>2u</sub> <sup>Bz</sup> → -s; 23% a → L+4 (1a <sub>2u</sub> <sup>*</sup> ); 14% H-12 (1b <sub>1u</sub> ) → -a; ...
				310 (4.00)	0.36	33% a → L+4 (1a <sub>2u</sub> <sup>*</sup> ); 26% 2a <sub>2u</sub> → -a; 10% 1a <sub>2u</sub> <sup>Bz</sup> → -s; ...
				309 (4.01)	0.49	30% a → L+4 (1a <sub>2u</sub> <sup>*</sup> ); 21% 2a <sub>2u</sub> → -a; ...
302 (4.11)	0.16	39% H-2 <sup>OAr</sup> → -a; 12% 1a <sub>2u</sub> <sup>Bz</sup> → -s; 12% H-8 <sup>OAr</sup> → -a; ...				
ZnPc4	723 (1.71) 678 (1.83)	0.64 0.6	97% a → -s; ... 97% a → -a; ...	364 (3.41)	0.16	35% H-1 <sup>Bz</sup> → -a; 27% a → L+2 (1b <sub>1u</sub> <sup>*</sup> ); 10% H-3 <sup>Bz</sup> → -a; ...
				361 (3.44)	0.42	31% H-2 <sup>Bz</sup> → -a; 21% a → L+2 (1b <sub>1u</sub> <sup>*</sup> ); 15% H-1 <sup>Bz</sup> → -a; ...
				341 (3.63)	0.4	84% H-3 <sup>Bz</sup> → -s; ...
				318 (3.90)	0.14	47% H-10 (2e <sub>g</sub> ) → -a; 16% H-4 <sup>OAr</sup> → -a; ...
				314 (3.95)	0.62	23% H-12 (1b <sub>1u</sub> ) → -a; 14% 2a <sub>2u</sub> → -a; 10% H-7 <sup>OAr</sup> → -a; ...
				312 (3.97)	0.23	28% H-4 <sup>OAr</sup> → -s; 15% 1a <sub>2u</sub> <sup>Bz</sup> → -a; 14% 2a <sub>2u</sub> → -a; ...
				310 (3.99)	0.41	17% H-4 <sup>OAr</sup> → -a; 12% H-5 <sup>OAr</sup> → -s; 10% 1a <sub>2u</sub> <sup>Bz</sup> → -s; ...
				305 (4.06)	0.35	48% H-7 <sup>OAr</sup> → -a; 27% 2a <sub>2u</sub> → -s; ...
				304 (4.08)	0.09	30% 1a <sub>2u</sub> <sup>Bz</sup> → -s; 29% H-6 <sup>OAr</sup> → -a; 19% H-14 (2e <sub>g</sub> ) → -a; ...
				299 (4.15)	0.07	23% H-12 (1b <sub>1u</sub> ) → -a; 14% 2a <sub>2u</sub> → -a; ...
297 (4.18)	0.08	29% H-6 <sup>OAr</sup> → -s; 18% 2a <sub>2u</sub> → -a; 12% 1a <sub>2u</sub> <sup>Bz</sup> → -s; ...				

<sup>a</sup>—The wavefunctions based on the eigenvectors predicted by sTD-DFT. One-electron transitions associated with the **a**, **-a** and **-s** MOs and the two frontier MOs derived from the 1a<sub>2u</sub> and 2a<sub>2u</sub> MOs of **ZnPc** that could potentially be viewed as the **s** MO are highlighted in bold. Only contributions > 10% to transitions with  $f > 0.10$  and  $\lambda > 285$  nm are consistently included. Bz, OAr and N as superscripts denote an MO that is mainly localized on the peripheral benzo rings, the peripheral OAr substituents and the aza-nitrogen lone pairs, respectively. Italics are used for other bands in the B band region (285–400 nm) that are not assigned to the main electronic B transitions in Figure 5. Where appropriate, the ZnPc MO from which the MO is derived is provided in parentheses.

The predicted energy gaps between the MOs of **ZnPc1–4** that are derived from the  $1a_{1u}$  and  $2a_{2u}$  MOs of the **ZnPc** parent complex are significantly smaller than is the case with **ZnPc\*** (Figure 4), since it is only the MOs derived from the  $1b_{1u}$  and  $1e_g$  MOs of **ZnPc** that are significantly destabilized by the presence of six or three diisopropylphenoxy groups in this context. As a result, multiple bands involving large contributions from the  $1a_{2u} \rightarrow a/-s$  and  $2a_{2u} \rightarrow a/-s$  one-electron transitions are predicted in the B band region in both the TD-DFT and sTD-DFT calculations (Tables 1 and 2). In contrast with the complexity of the calculated spectra of **ZnPc1–4** and **ZnPc\*** (Figure 5), only a relatively weak shoulder of absorbance is observed to the red of the main B band envelope in the experimental spectra (Figure 2). In a similar manner, only relatively minor differences are observed in the Faraday  $A_1$  and pseudo- $A_1$  terms in the B band regions of the MCD spectra of **ZnPc\*** and **ZnPc1–4** (Figure 2). These are likely to be associated with the large orbital angular momentum generated by transitions between the  $s$ ,  $-a$  and  $-s$  MOs with  $M_L = \pm 4$  and  $\pm 5$  angular nodal properties that are largely localized on the inner ligand perimeter [30,38,39]. The MCD spectra in Figure 2 therefore provide direct spectroscopic evidence that the TD-DFT and sTDDFT calculations in Figure 5 do not provide an accurate description of the B band region. In contrast with the relatively consistent Faraday  $A_1$  and pseudo- $A_1$  term band morphology that is observed in the B band region of the MCD spectra for **ZnPc\*** and **ZnPc1–4**, substantial differences are predicted in the wavefunctions in the B band region in Tables 1 and 2 and the simulated spectra in Figure 5. Extensive configurational interactions between a large number of  $\pi\pi^*$  excited states result in significant differences in the contributions from the  $1a_{2u} \rightarrow a/-s$  and  $2a_{2u} \rightarrow a/-s$  one-electron transitions which are highlighted in bold face in Tables 1 and 2.



**Figure 5.** Calculated spectra for **ZnPc**, **ZnPc\*** and **ZnPc1–4** derived from conventional TD-DFT (LEFT) and sTDDFT (RIGHT) calculations at the CAM-B3LYP/6-31G(d) level of theory. Q and B bands are highlighted with large red diamonds, while smaller amber, light blue, black, gray and green diamonds are used for bands arising primarily from transitions between destabilized  $\pi$ -MOs localized on the peripheral benzo rings into the  $-a/-s$  MOs, between the  $a$  MO into higher energy  $\pi^*$  MOs, between  $\sigma$ -MOs associated with the aza-nitrogen lone pairs into the  $-a/-s$  MOs, from MOs localized on the sterically demanding -OR substituents into the  $-a/-s$  MOs, and between other  $\pi$  MOs of the Pc ligands into the  $-a/-s$  MOs, respectively. Simulated spectra are derived from the Chemcraft [42] and Chemissian [43] programs, respectively, with a fixed bandwidth in each case of  $2000\text{ cm}^{-1}$ .

### 3. Discussion

The TD-DFT and sTD-DFT calculations (Figure 5, Tables 1 and 2) generally reproduce trends observed in the experimental spectra in the Q band region (Figures 2 and 5), which are often the most significant from the standpoint of applications such as DSSCs. The simplified approximation has the advantage of a spectacular speed-up in computation time,

but the mesomeric interactions of the carboxylic acid moieties are somewhat problematic in the context of the sTD-DFT calculations. The partial replacement of the electron-donating diisopropylphenoxy substituents of **ZnPc\*** with electron-withdrawing carboxylic acid groups and chlorine atoms (Figure 1) results in a stabilization of the energies of the frontier orbitals of **ZnPc1–4** (Figure 4). Lower molecular symmetry results in a lifting of the degeneracy of the -a and -s MOs. Larger  $\Delta$ LUMO values (Michl's terminology for the energy splitting of the -a and -s MOs [30]) are predicted for the dicarboxylic acid substituted **ZnPc2** and **ZnPc4** complexes, since there are large MO coefficients on the peripheral carbons of the B ring moiety of the -a MOs, but not on those of the -s MOs (Figure 3). The electron-withdrawing mesomeric interaction with the carboxylic acid groups is hence expected to stabilize the -a MOs relative to the -s MOs and result in separate *x*- and *y*-polarized  $Q_{00}$  bands.

Q band splittings of 29 and 59 nm are predicted for **ZnPc2** in the TD-DFT and sTD-DFT calculations (Tables 1 and 2), respectively, while smaller splittings of 23 and 45 nm are predicted for **ZnPc4** which has both a chlorine atoms and an isopropylphenoxy substituent on the A<sub>3</sub> benzo ring moieties. These bands are not resolved in the experimental spectra although significant broadening is observed in the  $Q_{00}$  bands of **ZnPc2** and **ZnPc4** relative to that of **ZnPc\*** (Figure 2). It is hence apparent that the extent of the Q band splitting associated with the mesomeric interactions with the carboxylic acid substituents is over-estimated in the sTD-DFT calculations of **ZnPc1–4**. This results in a significant under-estimation of the energies of the lower energy  $Q_{00}$  bands (Table 1). In contrast, there is a systematic over-estimation of the  $Q_{00}$  band energies in the TD-DFT calculations at the B3LYP/6-31G(d) level of theory (Table 2) as has been reported previously for calculations of this type for a wide range of different porphyrins and phthalocyanine-related structures [17,33,41,44,45].

Since the envisaged application for **ZnPc1–4** is in DSSCs as photosensitizer dyes coating the TiO<sub>2</sub> photoanode, a preliminary assessment of relevant parameters [46–50] was calculated on the basis of single point DFT calculations (Table 3) using the optimized geometries of the dyes at the B3LYP/SDD level of theory. Since the LUMO energies (Figure 6) are higher than that of the conduction band (CB) of TiO<sub>2</sub> [46,50], injection of an electron into the TiO<sub>2</sub> photoanode of the DSSC after photoexcitation should be feasible. Favorable open circuit voltage ( $V_{oc}$ ) values are predicted to lie in the 1.08–1.41 eV range for **ZnPc1–4** (Table 3). Spontaneous Gibbs free energies are predicted for the electron injection ( $\Delta G_{inj}$ ) and dye regeneration ( $\Delta G_{regen}$ ) processes shown in Figure 6 that are required to complete the circuit of the DSSC [46,50]. Favorable light-harvesting efficiency (LHE) values were also derived for the maxima of the Q bands using the oscillator strength (*f*) values from Table 1. Since these parameters appear to be promising, laboratory studies with DSSCs are already in progress to further assess the suitability of **ZnPc1–4** for this application.

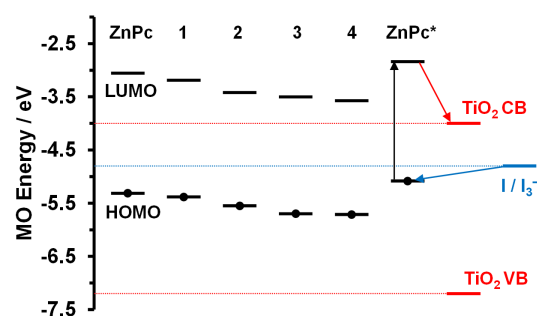


**Figure 6.** HOMO and LUMO energies for the B3LYP optimized geometries of **ZnPc**, **ZnPc\*** and **ZnPc1–4** at the B3LYP/SDD level of theory are plotted as black horizontal lines. Circles are used to highlight the HOMO in each case. Red lines are used to highlight the conduction band (CB) and valence band (VB) of TiO<sub>2</sub>, while a blue line is used for the redox potential of the I<sup>-</sup>/I<sub>3</sub><sup>-</sup> electrolyte [46,50]. Black, red and blue arrows are used to highlight the photoexcitation of the dye, injection of an electron into the TiO<sub>2</sub> CB, and regeneration of the dye, respectively, in the context of **ZnPc\***.

**Table 3.** Dye-sensitized solar cell (DSSC)-related parameters [46–50] for the B3LYP optimized geometries of **ZnPc**, **ZnPc\*** and **ZnPc1–4** at the B3LYP/SDD level of theory.

	HOMO (eV)	LUMO (eV)	Band gap (eV)	$E_{00}$ <sup>a</sup> (eV)	$E_{OX}^{dye}$ <sup>b</sup> (eV)	$E_{OX}^{dye*}$ <sup>c</sup> (eV)	$V_{oc}$ <sup>d</sup> (eV)	$\Delta G_{inj}$ <sup>e</sup> (eV)	$\Delta G_{regen}$ <sup>f</sup> (eV)	$f$ <sup>g</sup>	LHE <sup>h</sup>
<b>ZnPc</b>	−5.31	−3.05	2.26	1.86	5.31	3.46	1.01	−0.54	−0.51	0.48	0.67
<b>ZnPc1</b>	−5.38	−3.19	2.19	1.84	5.38	3.55	1.08	−0.45	−0.58	0.56	0.72
<b>ZnPc2</b>	−5.55	−3.42	2.13	1.83	5.55	3.72	1.25	−0.28	−0.75	0.56	0.72
<b>ZnPc3</b>	−5.70	−3.50	2.19	1.83	5.70	3.86	1.40	−0.14	−0.90	0.56	0.73
<b>ZnPc4</b>	−5.71	−3.58	2.14	1.82	5.71	3.89	1.41	−0.11	−0.91	0.57	0.73
<b>ZnPc*</b>	−5.08	−2.84	2.24	1.84	5.08	3.24	0.78	−0.76	−0.28	0.60	0.75

<sup>a</sup> The experimental Q band energy ( $E_{00}$ ) from Figure 2. <sup>b</sup> The oxidation potential of the dye ( $E_{OX}^{dye}$ ) is derived from the HOMO energy. <sup>c</sup> The oxidation potential of the photoexcited dye ( $E_{OX}^{dye*}$ ) is derived from the equation:  $E_{OX}^{dye*} = E_{OX}^{dye} - E_{00}$  [46,51]. <sup>d</sup> The open circuit voltage ( $V_{oc}$ ) values are calculated using the equation:  $V_{oc} = |E_{HOMO}(\text{Donor})| - |E_{LUMO}(\text{Acceptor})| - 0.3$  [46–49,51].  $|E_{HOMO}(\text{Donor})|$  and  $|E_{LUMO}(\text{Acceptor})|$  are derived from  $E_{OX}^{dye}$  and the energy of the conduction band of  $TiO_2$  ( $E_{CB}$ ) of  $-4.00$  eV [46,50]. <sup>e</sup> The Gibbs free energy for injection of an electron from the dye into the  $TiO_2$  photoanode ( $\Delta G_{inj}$ ) was calculated by using the equation:  $\Delta G_{inj} = E_{OX}^{dye*} - E_{CB}$  [46,51]. <sup>f</sup> The  $I/I_3^-$  redox potential of the electrolyte is assumed to be  $-4.80$  eV so the oxidation potential energy ( $E_{OX}^{electrolyte}$ ) is  $4.80$  eV [46,50] in the calculation of the Gibbs free energy for dye regeneration ( $\Delta G_{regen}$ ) using the equation:  $\Delta G_{regen} = E_{OX}^{electrolyte} - E_{OX}^{dye}$  [46]. <sup>g</sup> Average oscillator strength values for the Q transitions are derived from Table 1. <sup>h</sup> The light harvesting efficiency (LHE) at the Q band maxima was calculated using the equation:  $LHE = 1 - 10^{-f}$  [46,50,51].

## 4. Materials and Methods

### 4.1. Materials

The 4,5-bis(2,6-diisopropylphenoxy)phthalonitrile **1** [52], 4-chloro-5-(2,6-diisopropylphenoxy)phthalonitrile **2** [53], methyl-3,4-dicyanobenzoate **3** [54], and dimethyl-4,5-dicyanophthalate **4** [55,56] precursors were synthesized according to the previously reported procedures. Anhydrous zinc acetate was obtained by drying the corresponding dihydrate at  $90$  °C in vacuo. 1,8-Diazabicyclo[5.4.0]undec-7-ene (DBU, Aldrich) was vacuum distilled over  $CaH_2$  and stored under argon. Chloroform (puris) was distilled over  $CaH_2$ , *n*-pentanol (Aldrich) was distilled over  $Mg$  and stored under argon. Column chromatography was performed on silica (0.063–0.2 mm, Macherey-Nagel).

### 4.2. Methods

MALDI-TOF mass spectra were measured on a Bruker Daltonics Ultraflex mass spectrometer in positive ion mode with 2,5-dihydroxybenzoic acid (DHB) as a matrix. UV-visible absorption (UV-vis) spectra were recorded in  $CHCl_3$  on a Thermo Evolution 210 spectrometer in the 250–900 nm range. Rectangular quartz cuvettes with a 10 nm optical pathlength were used. NMR spectra were measured on a Bruker Avance-III spectrometer at a frequency of 600.13 MHz. Samples were prepared in  $CDCl_3$  (Cambridge Isotope Laboratories, Inc.), and filtered through a layer of alumina before use. Spectra were acquired at ambient temperatures. NMR spectra were referenced to the solvent signal ( $CHCl_3$ , 7.26 ppm). Magnetic circular dichroism (MCD) spectra were recorded with a Chirascan plus spectrometer (Applied Photophysics, UK) equipped with a 1.0 tesla permanent magnet by using both parallel and antiparallel fields.

### 4.3. Computational Details

Geometry optimizations were carried out for unsubstituted **ZnPc** (**ZnPc**) as a model complex, and **ZnPc\*** and **ZnPc1–4** at the B3LYP/6-31G(d) level of theory by using the Gaussian 09 software package [57]. Conventional TD-DFT calculations were carried out at the CAM-B3LYP/SDD level of theory since the CAM-B3LYP functional contains a long-range correction, while sTD-DFT calculations [21,22] were performed with the ORCA 5.0 package [58] using B3LYP/6-31G(d) optimized geometries. The MO energies and angular nodal patterns of **ZnPc**, **ZnPc\*** and **ZnPc1–4** were calculated at the CAM-B3LYP/6-31G(d)

level of theory [59–61]. The RIJCOSX approximation with auxiliary basis set def2/J was used to speed-up the sTD-DFT calculations [62,63]. Only the isomers shown for **ZnPc1–4** in Figure 4 are analysed in this study, since the calculated spectra of the other possible isomers were found to be broadly similar to those reported.

#### 4.4. Synthesis

**Zinc 2-carboxy-9,10,16,17,23,24-hexakis(2,6-diisopropylphenoxy)phthalocyaninate (ZnPc1).** A mixture of phthalonitrile **1** (300 mg, 0.6 mmol) and **3** (42 mg, 0.2 mmol), zinc acetate (76 mg, 0.4 mmol) and 1,8-diazabicyclo[5.4.0]undec-7-ene (DBU) (125  $\mu$ L, 0.8 mmol) in *n*-pentanol (5 mL) was degassed and refluxed under argon overnight. Then, *n*-pentanol was evaporated, and the dark-green sticky residue was sonicated with 50 vol. % aqueous EtOH, the precipitate was filtered, and washed with 50 vol. % aqueous ethanol. The dark-green solid was washed off the filter with chloroform. After solvent evaporation, this mixture of products was separated by column chromatography on silica through a gradient elution by a mixture of chloroform with hexane (30  $\rightarrow$  0 vol. %), then with methanol (0  $\rightarrow$  9 vol. %). The target (pentoxycarbonyl)phthalocyanine **ZnPcAm1** was eluted with a mixture containing 10 and 0 vol. % hexane, whereas some amounts of the hydrolysed product **ZnPc1** were eluted with a mixture containing 1–5 vol. % methanol. These fractions were combined, and the solvents were evaporated to give a dark green powder, which was used for hydrolysis without further purification.

The resulting product was mixed with a saturated aqueous sodium hydroxide solution (3 mL), dry tetrahydrofuran (3 mL), and methanol (10 mL). The solution was degassed and then heated to 40  $^{\circ}$ C with vigorous stirring under argon for 1.5 h. The hydrolysis was monitored by thin-layer chromatography (TLC) [silica, hexane/acetone, 1:1 (*v/v*)]. During the hydrolysis reaction, the  $R_f$  of the reaction mixture decreased to zero providing evidence for the production of the sodium salt of the target compound. The reaction mixture was then diluted with water (50 mL), acidified with concentrated hydrochloric acid to pH 3 and extracted with chloroform (3  $\times$  20 mL). Chloroform was evaporated from organic extracts, and the dark green residue was dried in vacuo. The **ZnPc1** target complex was isolated by column chromatography on silica, eluting with dichloromethane + 0 $\rightarrow$ 6 vol. % methanol, followed by size-exclusion chromatography on Bio-Beads SX-1 (isocratic elution with a chloroform–methanol 2.5 vol. % mixture). Dark-green powder. Yield: 66 mg, 17%. **ZnPcAm1:** MALDI TOF,  $m/z$  calcd for  $C_{110}H_{122}N_8O_8Zn$  1748.9, found 1748.5 [ $M^+$ ]. **ZnPc1:** MALDI TOF,  $m/z$  calcd for  $C_{105}H_{112}N_8O_8Zn$  1678.8, found 1678.5 [ $M^+$ ]. UV-vis (DMF),  $\lambda_{max}/nm$  (log  $\epsilon$ ) 261 (4.4), 288 (4.6), 359 (4.9), 612 (4.5), 678 (5.3).  $^1H$  NMR (600 MHz, Chloroform-*d* + 1/50 (*v/v*) pyridine-*d*<sub>5</sub>)  $\delta$  9.95 (s, 1H), 9.31 (d,  $J$  = 7.6 Hz, 1H), 8.84 (d,  $J$  = 6.9 Hz, 1H) ( $H'_{Pc}$ ,  $H''_{Pc}$ ,  $H'''_{Pc}$ ), 8.40 (d,  $J$  = 19.2 Hz, 2H), 8.20 (d,  $J$  = 8.6 Hz, 2H), 8.16 (d,  $J$  = 4.9 Hz, 2H) ( $H_{Pc}$ ), 7.56 (d,  $J$  = 7.8 Hz, 6H), 7.47 (d,  $J$  = 7.9 Hz, 10H), 7.38 (s, 2H) (*m,p*- $H_{OAr}$ ), 3.46 (q, 12H,  $H_{iPr}$ ), 1.36–1.23 (m, 72H,  $H_{Me}$ ).

**Zinc 2,3-dicarboxy-9,10,16,17,23,24-hexakis(2,6-diisopropylphenoxy)phthalocyaninate (ZnPc2).** The complex was synthesized by mixing phthalonitrile **1** (300 mg, 0.6 mmol) and **4** (54 mg, 0.2 mmol),  $Zn(OAc)_2$  (76 mg, 0.4 mmol) and DBU (0.13 mg, 0.8 mmol) in *n*-pentanol (5 mL) using the above-described procedure for **ZnPc1**. Dark green powder. Yield: 53 mg, 14%. **ZnPcAm2:** (MALDI TOF):  $m/z$  calcd for  $C_{116}H_{132}N_8O_{10}Zn$  1862.9, found 1862.8 [ $M^+$ ]. **ZnPc2:** MALDI TOF,  $m/z$  calcd for  $C_{106}H_{112}N_8O_{10}Zn$  1722.8, found 1722.4 [ $M^+$ ]. UV-vis (DMF),  $\lambda_{max}/nm$  (log  $\epsilon$ ) 289 (4.8), 360 (5.2), 615 (4.8), 682 (5.6).  $^1H$  NMR (300 MHz, Chloroform-*d* + 1/50 (*v/v*) pyridine-*d*<sub>5</sub>)  $\delta$  9.82 (s, 2H,  $H'_{Pc}$ ), 8.37 (s, 2H), 8.19 (s, 2H), 8.14 (s, 2H) ( $H_{Pc}$ ), 7.63–7.52 (m, 6H), 7.49–7.43 (m, 12H) (*m,p*- $H_{OAr}$ ), 3.46 (q,  $J$  = 6.1 Hz, 12H,  $H_{iPr}$ ), 1.28 (d,  $J$  = 21.7 Hz, 72H,  $H_{Me}$ ).

**Zinc 2-carboxy-9(10),16(17),23(24)-trichloro-10(9),17(16),24(23)-tris(2,6-diisopropylphenoxy) phthalocyaninate (ZnPc3).** The complex was synthesized starting from phthalonitriles **2** (300 mg, 0.9 mmol) and **3** (55 mg, 0.3 mmol),  $Zn(OAc)_2$  (110 mg, 0.6 mmol) and DBU (0.18 mg, 1.1 mmol) in *n*-pentanol (5 mL) using the above-described procedure for **ZnPc1**. Bluish-green powder. Yield: 56 mg, 15%. **ZnPcAm3:** MALDI TOF,

$m/z$  calcd for  $C_{74}H_{71}Cl_3N_8O_5Zn$  1324.3, found 1322.4  $[M^+]$ . **ZnPc3**: MALDI TOF  $m/z$  calcd for  $C_{69}H_{61}Cl_3N_8O_5Zn$  1252.3, found 1254.0  $[M^+]$ , 1276.0  $[M + Na - H]^+$ , 1292.0  $[M + K - H]^+$ . UV-vis (DMF):  $\lambda_{max}$  / nm (log  $\epsilon$ ): 283 (4.7), 357 (5.0), 612 (4.7), 679 (5.4).  $^1H$  NMR (600 MHz, Chloroform- $d$  + 1/50 ( $v/v$ ) pyridine- $d_5$ )  $\delta$  9.84 (s, 1H), 9.47 (m,  $J = 8.2$  Hz, 1H), 9.20 (s, 1H) ( $H'_{Pc}$ ,  $H''_{Pc}$ ,  $H'''_{Pc}$ ), 8.69 (s, 2H), 8.41 (s, 2H), 8.15 (s, 2H) ( $H^a_{Pc}$ ,  $H^b_{Pc}$ ), 7.57–7.53 (m, 3H), 7.49–7.43 (m, 6H) ( $m,p$ - $H_{OAr}$ ), 3.34–3.24 (m, 6H,  $H_{iPr}$ ), 1.40–1.14 (m, 36H,  $H_{Me}$ ).

**Zinc 2,3-dicarboxy-9(10),16(17),23(24)-trichloro-10(9),17(16),24(23)-tris(2,6-diisopropylphenoxy)phthalocyaninate (ZnPc4)**. The complex was synthesized starting from phthalonitriles **2** (300 mg, 0.9 mmol) and **4** (72 mg, 0.3 mmol),  $Zn(OAc)_2$  (110 mg, 0.6 mmol) and DBU (0.18 mg, 1.1 mmol) in  $n$ -pentanol (5 mL) using the above-described procedure for **ZnPc1**. Bluish-green powder. Yield: 74 mg, 19%. **ZnPcAm4**: MALDI TOF,  $m/z$  calcd for  $C_{80}H_{81}Cl_3N_8O_7Zn$  1437.5, found 1437.4  $[M^+]$ . **ZnPc4**: MALDI TOF,  $m/z$  calcd for  $C_{70}H_{61}Cl_3N_8O_7Zn$  1296.3, found 1297.6  $[M + H^+]$ . UV-vis (DMF):  $\lambda_{max}$  / nm (log  $\epsilon$ ): 284 (4.6), 356 (4.9), 618 (4.6), 683 (5.1).  $^1H$  NMR (600 MHz, DMSO- $d_6$ )  $\delta$  9.66–9.54 (m, 2H,  $H'_{Pc}$ ), 8.02 (s, 3H,  $H^a_{Pc}$ ), 7.73 (d,  $J = 7.6$  Hz, 3H), 7.63–7.56 (m, 6H) ( $m,p$ - $H_{OAr}$ ), 7.31 (s, 3H,  $H^b_{Pc}$ ), 1.32 (s, 36H,  $H_{Me}$ ).

**Zinc 2,3,9,10,16,17,23,24-octakis(2,6-di-isopropylphenoxy)phthalocyaninate (ZnPc\*)**. This product was obtained as a by-product in the synthesis of **ZnPc1** and **ZnPc2** as a green powder. MALDI TOF:  $m/z$  calcd for  $C_{128}H_{144}N_8O_8Zn$  1987.0, found 1986.7  $[M^+]$ . UV-vis (DMF),  $\lambda_{max}$ /nm (log  $\epsilon$ ): 288 (4.8), 359 (5.0), 611 (4.6), 677 (5.4).  $^1H$  NMR (300 MHz, Chloroform- $d$  + 1/50 ( $v/v$ )  $CD_3OD$ )  $\delta$  8.16 (s, 8H,  $H_{Pc}$ ), 7.60–7.51 (m, 8H,  $m$ - $H_{OAr}$ ), 7.47 (d,  $J = 8.3$  Hz, 16H,  $p$ - $H_{OAr}$ ), 3.47 (q,  $J = 6.8$  Hz, 16H,  $H_{iPr}$ ), 1.30 (s, 96H,  $H_{Me}$ ).

## 5. Conclusions

The rational design of novel phthalocyanine dyes for applications such as DSSCs is complicated by the challenging modelling calculations that are involved in the absence of access to a large computer cluster. This study demonstrates that the simplified sTD-DFT approach can rapidly provide useful information to predict or interpret the spectral trends observed in the Q band region of the UV-vis absorption spectra of  $\pi$ -extended chromophores such as **ZnPc1–4** and **ZnPc\***. However, it is noteworthy that the extent of the splitting of the Q band into  $x$ - and  $y$ -polarized components is over-estimated in the context of the lower symmetry **ZnPc1–4** complexes. It is clear from this series of test calculations for ZnPc complexes with peripheral substituents that introduce large mesomeric and inductive interactions with the  $\pi$ -system of the Pc ligand that the predictions made in the higher energy B band region in both TD-DFT and sTD-DFT calculations need to be treated cautiously. No significant extra insight is likely to be provided by the significantly longer calculation times associated with the conventional TD-DFT approach.

**Supplementary Materials:** The following supporting information can be downloaded. Figures S1–S5— $^1H$ -NMR spectra of synthesized complexes; Figures S6–S10—MALDI-TOF mass-spectra of synthesized complexes; Figures S11–S15—UV-vis spectra of synthesized complexes; Tables S1–S5—Cartesian coordinates of computed structures.

**Author Contributions:** Conceptualization, A.G.M. and Y.G.G.; Funding acquisition, Y.G.G. and T.N.; Investigation, D.A.B., N.N. and A.G.M.; Project administration, Y.G.G. and T.N.; Resources, J.M., Y.G.G. and T.N.; Visualization, A.G.M. and J.M.; Writing—original draft, D.A.B., A.G.M. and J.M.; Writing—review and editing, A.G.M., J.M., Y.G.G. and T.N. All authors have read and agreed to the published version of the manuscript.

**Funding:** This research was funded by the Russian Foundation for Basic Research (grant 19-53-60001) and the National Research Foundation of South Africa (uid: 118908/62620).

**Institutional Review Board Statement:** Not applicable.

**Informed Consent Statement:** Not applicable.

**Data Availability Statement:** Data is contained within the article or Supplementary Materials.

**Acknowledgments:** NMR and MALDI-TOF measurements were performed using the equipment of CKP FMI IPCE RAS and IGIC RAS. Theoretical calculations with the Gaussian 09 software package were carried out at the Centre for High Performance Computing in Cape Town.

**Conflicts of Interest:** The authors declare no conflict of interest.

**Sample Availability:** Samples of ZnPc1–4 are available from the authors.

## References

1. Lukyanets, E.A.; Nemykin, V.N. The key role of peripheral substituents in the chemistry of phthalocyanines and their analogs. *J. Porphyr. Phthalocyanines* **2010**, *14*, 1–40. [[CrossRef](#)]
2. Nyokong, T.; Ahsen, V. (Eds.) *Photosensitizers in Medicine, Environment, and Security*; Springer: Dordrecht, The Netherlands, 2012; ISBN 978-90-481-3870-8.
3. Koifman, O.I.; Ageeva, T.A.; Beletskaya, I.P.; Averin, A.D.; Yakushev, A.A.; Tomilova, L.G.; Dubinina, T.V.; Tsvadze, A.Y.; Gorbunova, Y.G.; Martynov, A.G.; et al. Macroheterocyclic Compound—a Key Building Block in New Functional Materials and Molecular Devices. *Macroheterocycles* **2020**, *13*, 311–467. [[CrossRef](#)]
4. Mack, J.; Kobayashi, N. Low symmetry phthalocyanines and their analogues. *Chem. Rev.* **2011**, *111*, 281–321. [[CrossRef](#)] [[PubMed](#)]
5. Urbani, M.; Ragoussi, M.E.; Nazeeruddin, M.K.; Torres, T.; Khaja, M. Phthalocyanines for dye-sensitized solar cells. *Coord. Chem. Rev.* **2019**, *381*, 1–64. [[CrossRef](#)]
6. Cid, J.J.; Yum, J.H.; Jang, S.R.; Nazeeruddin, M.K.; Martínez-Ferrero, E.; Palomares, E.; Ko, J.; Grätzel, M.; Torres, T. Molecular cosensitization for efficient panchromatic dye-sensitized solar cells. *Angew. Chem. Int. Ed.* **2007**, *46*, 8358–8362. [[CrossRef](#)]
7. Tortelli, S.; Cavazzini, M.; Orlandi, S.; Pozzi, G.; Pecnikaj, I.; Caramori, S.; Boaretto, R. Property tuning in unsymmetrical alkoxy zinc phthalocyanines by introduction of perfluoro-tert-butoxy end groups. *J. Fluor. Chem.* **2016**, *188*, 110–116. [[CrossRef](#)]
8. Ikeuchi, T.; Mori, S.; Kobayashi, N.; Kimura, M. Low-Symmetrical Zinc(II) Benzonaphthoporphyrizine Sensitizers for Light-Harvesting in Near-IR Region of Dye-Sensitized Solar Cells. *Inorg. Chem.* **2016**, *55*, 5014–5018. [[CrossRef](#)]
9. Ikeuchi, T.; Nomoto, H.; Masaki, N.; Griffith, M.J.; Mori, S.; Kimura, M. Molecular engineering of zinc phthalocyanine sensitizers for efficient dye-sensitized solar cells. *Chem. Commun.* **2014**, *50*, 1941. [[CrossRef](#)]
10. Kimura, M.; Nomoto, H.; Suzuki, H.; Ikeuchi, T.; Matsuzaki, H.; Murakami, T.N.; Furube, A.; Masaki, N.; Griffith, M.J.; Mori, S. Molecular Design Rule of Phthalocyanine Dyes for Highly Efficient Near-IR Performance in Dye-Sensitized Solar Cells. *Chem.-A Eur. J.* **2013**, *19*, 7496–7502. [[CrossRef](#)]
11. Virkki, K.; Hakola, H.; Urbani, M.; Tejerina, L.; Ince, M.; Martínez-Díaz, M.V.; Torres, T.; Golovanova, V.; Golovanov, V.; Tkachenko, N.V. Photoinduced Electron Injection from Zinc Phthalocyanines into Zinc Oxide Nanorods: Aggregation Effects. *J. Phys. Chem. C* **2017**, *121*, 9594–9605. [[CrossRef](#)]
12. Nombona, N.; Antunes, E.; Litwinski, C.; Nyokong, T. Synthesis and photophysical studies of phthalocyanine-gold nanoparticle conjugates. *Dalton Trans.* **2011**, *40*, 11876. [[CrossRef](#)]
13. Ballesteros, B.; Campidelli, S.; de la Torre, G.; Ehli, C.; Guldi, D.M.; Prato, M.; Torres, T. Synthesis, characterization and photophysical properties of a SWNT-phthalocyanine hybrid. *Chem. Commun.* **2007**, 2950. [[CrossRef](#)]
14. Yang, L.; Guo, L.; Chen, Q.; Sun, H.; Liu, J.; Zhang, X.; Pan, X.; Dai, S. Theoretical design and screening of panchromatic phthalocyanine sensitizers derived from TT1 for dye-sensitized solar cells. *J. Mol. Graph. Model.* **2012**, *34*, 1–9. [[CrossRef](#)]
15. Milan, R.; Selopal, G.S.; Cavazzini, M.; Orlandi, S.; Boaretto, R.; Caramori, S.; Concina, I.; Pozzi, G. Dye-sensitized solar cells based on a push-pull zinc phthalocyanine bearing diphenylamine donor groups: Computational predictions face experimental reality. *Sci. Rep.* **2017**, *7*, 1–10. [[CrossRef](#)] [[PubMed](#)]
16. Milan, R.; Singh Selopal, G.; Cavazzini, M.; Orlandi, S.; Boaretto, R.; Caramori, S.; Concina, I.; Pozzi, G. Zinc phthalocyanines as light harvesters for SnO<sub>2</sub>-based solar cells: A case study. *Sci. Rep.* **2020**, *10*, 1–9. [[CrossRef](#)] [[PubMed](#)]
17. Mack, J.; Bunya, M.; Shimizu, Y.; Uoyama, H.; Komobuchi, N.; Okujima, T.; Uno, H.; Ito, S.; Stillman, M.J.; Ono, N.; et al. Application of MCD spectroscopy and TD-DFT to nonplanar core-modified tetrabenzoporphyrins: Effect of reduced symmetry on nonplanar porphyrinoids. *Chem. Eur. J.* **2008**, *14*, 5001–5020. [[CrossRef](#)] [[PubMed](#)]
18. Hoshi, T.; Kobayashi, N. Spectroscopic and structural properties of phthalocyanines deduced from their frontier molecular orbitals (MOs) and MO calculations. *Coord. Chem. Rev.* **2017**, *345*, 31–41. [[CrossRef](#)]
19. Nemykin, V.N.; Hadt, R.G.; Belosludov, R.V.; Mizuseki, H.; Kawazoe, Y. Influence of Molecular Geometry, Exchange-Correlation Functional, and Solvent Effects in the Modeling of Vertical Excitation Energies in Phthalocyanines Using Time-Dependent Density Functional Theory (TDDFT) and Polarized Continuum Model TDDFT Methods: Ca. *J. Phys. Chem. A* **2007**, *111*, 12901–12913. [[CrossRef](#)] [[PubMed](#)]
20. Belosludov, R.V.; Nevonen, D.; Rhoda, H.M.; Sabin, J.R.; Nemykin, V.N. Simultaneous Prediction of the Energies of Q<sub>x</sub> and Q<sub>y</sub> Bands and Intramolecular Charge-Transfer Transitions in Benzoannulated and Non-Peripherally Substituted Metal-Free Phthalocyanines and Their Analogues: No Standard TDDFT Silver Bullet Yet. *J. Phys. Chem. A* **2019**, *123*, 132–152. [[CrossRef](#)] [[PubMed](#)]
21. Bannwarth, C.; Grimme, S. A simplified time-dependent density functional theory approach for electronic ultraviolet and circular dichroism spectra of very large molecules. *Comput. Theor. Chem.* **2014**, *1040–1041*, 45–53. [[CrossRef](#)]

22. Martynov, A.G.; Mack, J.; May, A.K.; Nyokong, T.; Gorbunova, Y.G.; Tsivadze, A.Y. Methodological Survey of Simplified TD-DFT Methods for Fast and Accurate Interpretation of UV-Vis-NIR Spectra of Phthalocyanines. *ACS Omega* **2019**, *4*, 7265–7284. [[CrossRef](#)] [[PubMed](#)]
23. Safonova, E.A.; Martynov, A.G.; Polovkova, M.A.; Ugolkova, E.A.; Minin, V.V.; Gorbunova, Y.G.; Tsivadze, A.Y. 5,8-Disubstituted crown-naphthalonitriles as a platform for highly soluble naphthalocyanines. *Dye. Pigment.* **2020**, *180*, 108484. [[CrossRef](#)]
24. Yagodin, A.V.; Martynov, A.G.; Gorbunova, Y.G.; Tsivadze, A.Y. Synthesis, electronic structure and NH-tautomerism of novel mono- and dibenzoannelated phthalocyanines. *Dye. Pigment.* **2020**, *181*, 108564. [[CrossRef](#)]
25. May, A.; Majumdar, P.; Martynov, A.G.; Lapkina, L.A.; Troyanov, S.I.; Gorbunova, Y.G.; Tsivadze, A.Y.; Mack, J.; Nyokong, T. Optical limiting properties, structure and simplified TD-DFT calculations of scandium tetra-15-crown-5 phthalocyaninates. *J. Porphyr. Phthalocyanines* **2020**, *24*, 589–601. [[CrossRef](#)]
26. Tejerina, L.; Martínez-Díaz, M.V.; Torres, T. Convergent Strategy for the Regioselective Synthesis of Nonaggregated  $\alpha$ -Triaryl- $\beta$ -carboxy Zinc Phthalocyanines. *Org. Lett.* **2015**, *17*, 552–555. [[CrossRef](#)]
27. Listorti, A.; López-Duarte, I.; Martínez-Díaz, M.V.; Torres, T.; DosSantos, T.; Barnes, P.R.F.; Durrant, J.R. Zn(ii) versus Ru(ii) phthalocyanine-sensitized solar cells. A comparison between singlet and triplet electron injectors. *Energy Environ. Sci.* **2010**, *3*, 1573–1579. [[CrossRef](#)]
28. Aktas, E.; Jiménez-López, J.; Azizi, K.; Torres, T.; Palomares, E. Self-assembled Zn phthalocyanine as a robust p-type selective contact in perovskite solar cells. *Nanoscale Horiz.* **2020**, *5*, 1415–1419. [[CrossRef](#)]
29. Gouterman, M. Optical Spectra and Electronic Structure of Porphyrins and Related Rings. In *The Porphyrins*; Dolphin, D., Ed.; Academic Press: New York, NY, USA, 1978; Volume III, pp. 1–165.
30. Michl, J. Magnetic circular dichroism of aromatic molecules. *Tetrahedron* **1984**, *40*, 3845–3934. [[CrossRef](#)]
31. Schaffer, A.M.; Gouterman, M.; Davidson, E.R. Porphyrins XXVIII. Extended Hückel calculations on metal phthalocyanines and tetrazaporphins. *Theor. Chim. Acta* **1973**, *30*, 9–30. [[CrossRef](#)]
32. McHugh, A.J.; Gouterman, M.; Weiss, C. Porphyrins XXIV. Energy, oscillator strength, and Zeeman splitting calculations (SCMO-CI) for phthalocyanine, porphyrins, and related ring systems. *Theor. Chim. Acta* **1972**, *24*, 346–370. [[CrossRef](#)]
33. Mack, J.; Wildervanck, M.; Nyokong, T. TD-DFT calculations and MCD spectroscopy of porphyrin and phthalocyanine analogues: Rational design of photosensitizers for PDT and NIR region sensor applications. *Turk. J. Chem.* **2014**, *38*, 1013–1026. [[CrossRef](#)]
34. Nyokong, T.; Gasyna, Z.; Stillman, M.J. Analysis of the absorption and magnetic circular dichroism spectra of zinc phthalocyanine and the pi-cation-radical species [ZnPc(1-)]<sup>•+</sup>. *Inorg. Chem.* **1987**, *26*, 1087–1095. [[CrossRef](#)]
35. Ough, E.; Nyokong, T.; Creber, K.A.M.; Stillman, M.J. Electrochemistry and Spectroscopy of Magnesium Phthalocyanine. Analysis of the Absorption and Magnetic Circular Dichroism Spectra. *Inorg. Chem.* **1988**, *27*, 2724–2732. [[CrossRef](#)]
36. Stillman, M.J.; Nyokong, T. Absorption and Magnetic Circular Dichroism Spectral Properties of Phthalocyanines. Part 1: Complexes of the Dianion, Pc(-2). In *Phthalocyanines: Properties and Applications 1*; Leznoff, C.C., Lever, A.B.P., Eds.; VCH: Weinheim, Germany, 1989; pp. 133–289.
37. Mack, J.; Stillman, M.J. Electronic Structures of Metal Phthalocyanine and Porphyrin Complexes from Analysis of the UV-Visible Absorption and Magnetic Circular Dichroism Spectra and Molecular Orbital Calculations. In *The Porphyrin Handbook*; Kadish, K.M., Smith, K.M., Guillard, R., Eds.; Academic Press: New York, NY, USA, 2003; pp. 43–116.
38. Mack, J.; Stillman, M.J.; Kobayashi, N. Application of MCD spectroscopy to porphyrinoids. *Coord. Chem. Rev.* **2007**, *251*, 429–453. [[CrossRef](#)]
39. Kobayashi, N.; Nakai, K. Applications of magnetic circular dichroism spectroscopy to porphyrins and phthalocyanines. *Chem. Commun.* **2007**, 4077. [[CrossRef](#)]
40. Isago, H. *Optical Spectra of Phthalocyanines and Related Compounds A Guide for Beginners*; Springer: Berlin/Heidelberg, Germany, 2015; ISBN 978-4-431-55101-0.
41. Mack, J.; Asano, Y.; Kobayashi, N.; Stillman, M.J. Application of MCD spectroscopy and TD-DFT to a highly non-planar porphyrinoid ring system. New insights on red-shifted porphyrinoid spectral bands. *J. Am. Chem. Soc.* **2005**, *127*, 17697–17711. [[CrossRef](#)] [[PubMed](#)]
42. Chemcraft-Graphical Software for Visualization of Quantum Chemistry Computations. Available online: <https://www.chemcraftprog.com> (accessed on 12 December 2021).
43. Chemissian 4.65 Program (by L. Skripnikov). Available online: <https://www.chemissian.com/> (accessed on 12 December 2021).
44. Mack, J. Expanded, Contracted, and Isomeric Porphyrins: Theoretical Aspects. *Chem. Rev.* **2017**, *117*, 3444–3478. [[CrossRef](#)]
45. Lu, H.; Mack, J.; Yang, Y.; Shen, Z. Structural modification strategies for the rational design of red/NIR region BODIPYs. *Chem. Soc. Rev.* **2014**, *43*, 4778–4823. [[CrossRef](#)] [[PubMed](#)]
46. Yasseen, F.A.; Al-Temime, F.A. Electronic structures and photovoltaic properties of a novel phthalocyanine and titanium dioxide phthalocyanine for dye sensitized-solar cells. *GSC Adv. Res. Rev.* **2021**, *6*, 107–115. [[CrossRef](#)]
47. Xiang, Y.; Zhang, J.; Zheng, S. Designing Potential Donor Materials Based on DRCN5T with Halogen Substitutions: A DFT/TDDFT Study. *Int. J. Mol. Sci.* **2021**, *22*, 13498. [[CrossRef](#)]
48. Scharber, M.C.; Mühlbacher, D.; Koppe, M.; Denk, P.; Waldauf, C.; Heeger, A.J.; Brabec, C.J. Design Rules for Donors in Bulk-Heterojunction Solar Cells—Towards 10% Energy-Conversion Efficiency. *Adv. Mater.* **2006**, *18*, 789–794. [[CrossRef](#)]
49. Bourass, M.; Benjelloun, A.T.; Benzakour, M.; Mcharfi, M.; Hamidi, M.; Bouzzine, S.M.; Bouachrine, M. DFT and TD-DFT calculation of new thienopyrazine-based small molecules for organic solar cells. *Chem. Cent. J.* **2016**, *10*, 67. [[CrossRef](#)] [[PubMed](#)]

50. Lu, X.; Wei, S.; Wu, C.-M.; Li, S.; Guo, W. Can Polypyridyl Cu(I)-based Complexes Provide Promising Sensitizers for Dye-Sensitized Solar Cells? A Theoretical Insight into Cu(I) versus Ru(II) Sensitizers. *J. Phys. Chem. C* **2011**, *115*, 3753–3761. [[CrossRef](#)]
51. Juma, J.M.; Vuai, S.A.H.; Babu, N.S. TD-DFT Investigations on Optoelectronic Properties of Fluorescein Dye Derivatives in Dye-Sensitized Solar Cells (DSSCs). *Int. J. Photoenergy* **2019**, *2019*, 1–8. [[CrossRef](#)]
52. Toriumi, N.; Muranaka, A.; Hirano, K.; Yoshida, K.; Hashizume, D.; Uchiyama, M.  $18\pi$ -Electron Tautomeric Benzophthalocyanine: A Functional Near-Infrared Dye with Tunable Aromaticity. *Angew. Chem. Int. Ed.* **2014**, *53*, 7814–7818. [[CrossRef](#)]
53. Anderson, D.R.; Solntsev, P.V.; Rhoda, H.M.; Nemykin, V.N. How big is big? Separation by conventional methods, X-ray and electronic structures of positional isomers of bis-tert-butylisocyanide adduct of 2(3),9(10),16(17),23(24)-tetrachloro-3(2),10(9),17(16),24(23)-tetra(2,6-di-iso-propylphenoxy)-phthalocyanine. *J. Porphyr. Phthalocyanines* **2016**, *20*, 337–351. [[CrossRef](#)]
54. Pozzi, G.; Quici, S.; Raffo, M.C.; Bignozzi, C.A.; Caramori, S.; Orlandi, M. Fluorous molecules for dye-sensitized solar cells: Synthesis and photoelectrochemistry of unsymmetrical zinc phthalocyanine sensitizers with bulky fluorophilic donor groups. *J. Phys. Chem. C* **2011**, *115*, 3777–3788. [[CrossRef](#)]
55. Shimizu, M.; Tamagawa, T. Design and Characterization of 4,5-Bis(diarylamino)phthalic Acid Diesters as a New Class of Fluorophores Exhibiting Efficient Blue Emission in the Solid State. *Eur. J. Org. Chem.* **2015**, *2015*, 291–295. [[CrossRef](#)]
56. Tylleman, B.; Gómez-Aspe, R.; Gbabode, G.; Geerts, Y.H.; Sergeyev, S. Ester-functionalized phthalonitriles and zinc phthalocyanines via palladium-catalyzed cyanation of 4,5-dichlorophthalates. *Tetrahedron* **2008**, *64*, 4155–4161. [[CrossRef](#)]
57. Frisch, M.J.; Trucks, G.W.; Schlegel, H.B.; Scuseria, G.E.; Robb, M.A.; Cheeseman, J.R.; Montgomery, J.A., Jr.; Vreven, T.; Kudin, K.N.; Burant, J.C.; et al. *Gaussian 03, Revision E.01*; Gaussian Inc.: Wallingford, CT, USA, 2004.
58. Neese, F. Software update: The ORCA program system, version 4.0. *Wiley Interdiscip. Rev. Comput. Mol. Sci.* **2018**, *8*, e1327. [[CrossRef](#)]
59. Yanai, T.; Tew, D.P.; Handy, N.C. A new hybrid exchange–correlation functional using the Coulomb-attenuating method (CAM-B3LYP). *Chem. Phys. Lett.* **2004**, *393*, 51–57. [[CrossRef](#)]
60. Hehre, W.J.; Ditchfield, R.; Pople, J.A. Self-Consistent Molecular Orbital Methods. XII. Further Extensions of Gaussian-Type Basis Sets for Use in Molecular Orbital Studies of Organic Molecules. *J. Chem. Phys.* **1972**, *56*, 2257. [[CrossRef](#)]
61. Rassolov, V.A.; Pople, J.A.; Ratner, M.A.; Windus, T.L. 6-31G \* basis set for atoms K through Zn. *J. Chem. Phys.* **1998**, *109*, 1223–1229. [[CrossRef](#)]
62. Izsák, R.; Neese, F. An overlap fitted chain of spheres exchange method. *J. Chem. Phys.* **2011**, *135*, 144105. [[CrossRef](#)] [[PubMed](#)]
63. Weigend, F. Accurate Coulomb-fitting basis sets for H to Rn. *Phys. Chem. Chem. Phys.* **2006**, *8*, 1057–1065. [[CrossRef](#)] [[PubMed](#)]